ELSEVIER

Remote Sensing of Environment 84 (2003) 192–207

Remote Sensing of Environment

www.elsevier.com/locate/rse

Optimum pixel size for hyperspectral studies of ecosystem function in southern California chaparral and grassland

Abdullah F. Rahman *, John A. Gamon, Daniel A. Sims, Miriam Schmidts

Biology and Microbiology Department, California State University, 5151 State University Drive, Los Angeles, CA 90032, USA

Received 26 February 2001; received in revised form 31 May 2002; accepted 16 June 2002

Abstract

Hyperspectral remotely sensed data are useful for studying ecosystem processes and patterns. However, spatial characterization of such remotely sensed images is needed to optimize sampling procedures and address scaling issues. We have investigated spatial scaling in ground-based and airborne hyperspectral data for canopy- to watershed-level ecosystem studies of southern California chaparral and grassland vegetation. Three optical reflectance indices, namely, Normalized Difference Vegetation Index (NDVI), Water Band Index (WBI) and Photochemical Reflectance Index (PRI) were used as indicators of biomass, plant water content and photosynthetic activity, respectively. Two geostatistical procedures, the semivariogram and local variance, were used for the spatial scaling analysis of these indices. The results indicate that a pixel size of 6 m or less would be optimal for studying functional properties of southern California grassland and chaparral ecosystems using hyperspectral remote sensing. These results provide a guide for selecting the spatial resolution of future airborne and satellite-based hyperspectral sensors.

1. Introduction

Spatial heterogeneity is inherent in natural vegetation. Key vegetation physiological and physical processes occur over a wide range of spatial scales, ranging from individual molecules to leaves, canopy, local and global scales. The relationships of these physical and physiological processes are often nonlinear (Hari et al., 1984; Lappi & Smolander, 1984), and extraction of ecologically meaningful information may depend on the spatial scale at which data are collected (Jarvis & McNaughton, 1986). Earth scientists are constrained by the predetermined spatial resolution (i.e., the pixel size) of the satellite imagery when using satellite-based remotely sensed data. For the last couple of decades, ecologists and earth scientists have used Landsat images at 30-m pixel size, or NOAA-AVHRR images at 1.1-km pixel size, to derive information that may have spatial variance smaller than those pixels. Spectral mixture modeling and other techniques have been applied to derive sub-pixel information hidden in a larger pixel (Roberts, Green, & Adams, 1997; Ustin et al., 1998). As environmental remote sensing matures, ecologists and Earth scientists need to specify the proper spatial scale and pixel sizes needed for studying different aspects of ecosystems, so that engineers can develop the corresponding space- or aircraft-based systems suited for those purposes.

Spectral information of vegetated surfaces contained in a pixel of remotely sensed data varies with sensor geometry and platform height (Curran & Guyot, 1997). Depending on the field of view (FOV) of the sensor, a handheld spectrometer at 1 m above a canopy generally 'sees' a couple of square centimeters to a square meter area as its pixel size. Airborne sensors (e.g. Airborne Visible Infrared Imaging Spectrometer or AVIRIS, Green et al., 1998) and spaceborne sensors (e.g. Moderate Resolution Imaging Spectrometer, or MODIS) generally have pixel sizes ranging from tens of meters to kilometers. Therefore, reflectance recorded from a handheld spectrometric pixel, with an area of a few square centimeters from a natural area would not be directly comparable to an image pixel with an area ranging from a few square meters to couple of square kilometers collected from the same general area using AVIRIS or MODIS. To compare handheld spectral data to aerial and satellite imagery, or

* Corresponding author. Current address: Room #CL 425, Geography Department, Ball State University, Muncie, IN 47306, USA. Tel.: +1-765-285-1172; fax: +1-765-285-2351.

E-mail address: faiz@bsu.edu (A.F. Rahman).

0034-4257/02/$ - see front matter © 2002 Elsevier Science Inc. All rights reserved.
PII: S0034-4257(02)00107-4

to use satellite imagery for deriving surface processes at smaller spatial resolutions, the issue of spatial scaling has to be addressed.

As defined by Jarvis (1995), the scaling process involves "taking information at one scale and using it to derive processes at another scale." Upscaling is the process of taking information at smaller spatial resolutions (such as handheld spectrometric data) and deriving information at larger spatial resolutions (such as AVIRIS or MODIS pixels). Downscaling involves the decomposition of data collected at larger spatial resolutions into information at smaller spatial resolutions.

As part of a larger study of multi-scale ecosystem function in chaparral and grassland of the Santa Monica Mountains region in southern California, we have been examining the suitability of different hyperspectral sensors and platforms. Previous studies have shown that hyperspectral remote sensing can potentially increase the accuracy of ecosystem process models by providing model inputs based on fundamental biophysical properties linked to physiological function (Gamon & Qiu 1999; Roberts et al., 1997; Ustin et al., 1998). Water and pigment absorption features in vegetation are two physiologically relevant signals that are detectable based on reflectance features present in hyperspectral data (Fillela, Amaro, & Peñuelas, 1996; Gamon et al., 1998; Peñuelas, Filella, Biel, Serrano, & Save, 1993; Peñuelas, Filella, & Gamon, 1995; Peñuelas, Pinol, Ogaya, & Filella, 1997). Green biomass and green leaf area index are linked to vegetation indices calculated from reflectance at visible and near infrared regions (Gamon, Green, Roberts, & Serrano, 1995; Goward & Huemmrich, 1992).

The objective of this paper is to examine the spatial characteristics of hyperspectral signatures from chaparral and grassland vegetation in southern California to determine an optimum pixel size for landscape level ecosystem studies. Biomass, photosynthetic activity and vegetation water content are used in this study as indicators of ecosystem function that could be estimated using hyperspectral remote sensing. A proper understanding of spatial dependence of these variables is essential to avoid the potential errors arising from heterogeneity and patchiness in upscaling or downscaling physiological processes. We adopt the geostatistical methods of semivariogram analysis and local variance analysis with ground-based hyperspectral data and AVIRIS imagery for this purpose.

2. Relevance of geostatistics

2.1. Spectral reflectance and semivariograms

Surface reflectance in a given spectral waveband is a spatially continuous variable at the pixel size of a given sensor. In geostatistics, such an attribute with spatial continuity is called a *regionalized variable* (Matheron, 1971). The second-order spatial characteristics of a regionalized variable are modeled in geostatistics by the semivariogram (Cohen, Spies, & Bradshaw, 1990; Curran, 1988; McBratney & Webster, 1986). One objective of this study is to investigate the spatial variances of hyperspectral reflectance products with semivariograms.

To relate semivariogram analysis to the sampling method used in this study, we can imagine a transect running across an area, where the surface reflectance values have been collected at pixels in regular intervals (Fig. 1A). The spatial variance between reflectance values of any two distinct pixels would depend on their separation distance h (called "lag"). The semivariance, $\gamma(h)$, of reflectance values between any two pixels at a lag of h can be expressed as:

$$\gamma(h) = \frac{1}{2}[z(x) - z(x+h)]^2 \quad (1)$$

where $z(x)$ is the reflectance value at a pixel with coordinate vector ($\boldsymbol{x}$). For simplicity we denote x as a scalar. There will be $n(h)$ pairs of observations within the transect

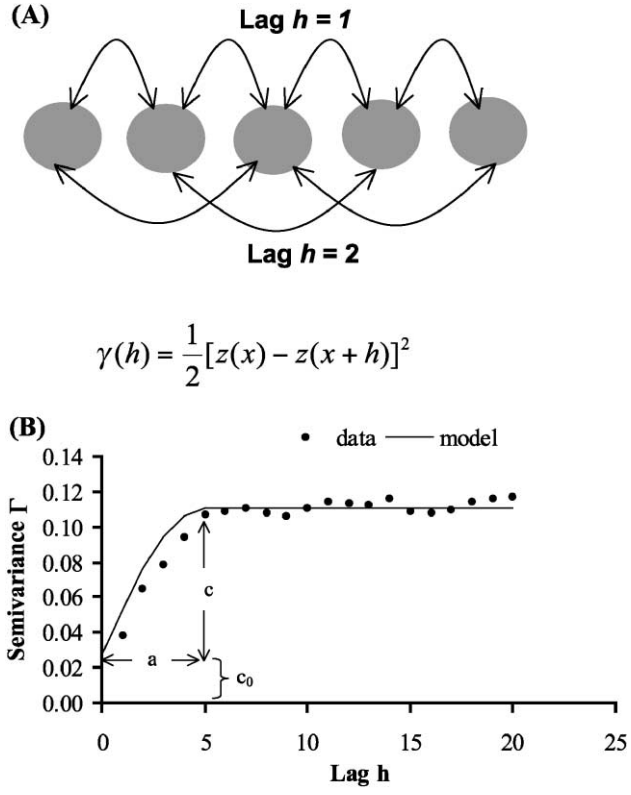

Fig. 1. (A) A schematic diagram of semivariance between different lags along a transect of data points. Lags of 1 and 2 pixels are shown along with the formulation of semivariance for any lag h. (B) A spherical semivariogram showing range (a), sill (c) and nugget (c_0). The dots represent experimental data and the solid line represents the model fit.

separated by a particular lag h. Their semivariance is given by:

$$\Gamma(h) = \frac{1}{2n}\sum_{i=1}^{n}[z(x_i) - z(x_i + h)]^2 \quad (2)$$

Here, $\Gamma(h)$ is an unbiased estimate of the population variance, and is a useful measure of dissimilarity between spatially distributed regionalized variables. The larger $\Gamma(h)$, the less similar the pixels. The relationship between semivariance (Γ) and different lag vectors h provides a semivariogram for the population.

When a semivariogram is plotted using discrete experimental data points, it is called an experimental or sample semivariogram. However, to quantify spatial patterns, or to optimize sampling, it is necessary to fit a theoretical model through the experimental data points. Three key model terms are: (1) sill, (2) range and (3) nugget variance (Fig. 1B). The sill is the theoretical maximum variance of the semivariogram and as such represents the inherent variance of the regionalized attribute. The range is the lag of semivariogram at which the sill is attained and marks the limit of spatial dependence of that attribute. The nugget variance is the positive intercept of the semivariogram and can be caused by measurement errors or unexplained sub-pixel variance present in the data.

For this research, we applied one semivariogram model commonly used for natural system studies (McBratney & Webster, 1981; Webster & Nortcliff, 1984). It is called the spherical model, and is expressed as:

$$\begin{cases} \Gamma(h) = c_0 & \text{when } h = \varepsilon \text{ (a very small lag)} \\ \Gamma(h) = c_0 + c\left(\dfrac{3h}{2a} - \dfrac{h^3}{2a^3}\right) & \text{when } 0 < h \le a \\ \Gamma(h) = c_0 + c & \text{when } h > a \end{cases} \quad (3)$$

where c_0 is the nugget variance, c is the sill, h is the lag and a is the range. The gradient of the spherical function is $3c/2a$ till it reaches the sill. It becomes zero at sill and the function becomes a straight line (Fig. 1B). The sill of the semivariogram corresponds to the estimate of true variance of the data. The corresponding range denotes the distance at which the samples become spatially uncorrelated.

The most important factor for this study was the range of the semivariogram, which would indicate the size of objects in the landscape. According to sampling theorems, to effectively sample objects, one must sample at least at one-half the width of the object (McGrew & Monroe, 2000). Therefore, for remote sensing purposes, a spatial resolution element (or pixel) smaller than or equal to half the semivariogram range would be an appropriate one to study the spatially distributed characteristics of that surface. This would define the distance above which spatial resolution elements are not related (Curran, 1988). For example, for a vegetated landscape, this might be related to functionally distinct species or vegetation types, or the difference between vegetation and bare ground. To capture the distinct functional properties of components in such a landscape, it is then advisable to choose a pixel size that is smaller than or equal to half the range of the semivariogram.

2.2. Fitting semivariogram models

Model fitting is one of the basic problems in using semivariograms for spatial studies. Deriving the appropriate sill, range and nugget from the discrete experimental data is essential for fitting the continuous semivariogram model. Methods of model fitting range in practice from simple visual fitting to complex mathematical algorithms. Even though the visual fitting is practiced in many cases, it is not advisable because it does not have any theoretical basis and one person's visual fit may not be same as another person's (McBratney & Webster, 1981).

Most of the mathematical model-fitting techniques work well, but they involve complex algorithms. Recently, Chen and Jiao (2000) have introduced a method of estimating the parameters of six different semivariogram models by simple linear programming techniques. They used the theory of nonnegative solution of linear equations for this purpose. Since our paper uses only the spherical model, we briefly discuss here how the parameters of a spherical model can be derived using a linear solution.

According to the model described in Eq. (3), when $h = \varepsilon$ or $h > a$, $\Gamma(h)$ is equal to c_0 and $(c_0 + c)$, respectively. Therefore, a solution of $\Gamma(h)$ when $\varepsilon < h \le a$ would solve the problem. When $\varepsilon < h \le a$, Eq. (3) can be written as:

$$\Gamma(h) = c_0 + \left(\frac{3c}{2a}\right)h + \left(\frac{-c}{2a^3}\right)h^3 \quad (4)$$

Replacing b, x_2, x_3, a_1, a_2 and a_3 for $\Gamma(h)$, $3c/2a$, $-c/2a^3$, c_0, h and h^3, respectively, and defining a new variable $x_1 = 1$, we get the following linear equation:

$$b = a_1x_1 + a_2x_2 + a_3x_3 \quad (5)$$

Let $h_1, h_2, \ldots h_n$ denote $n(h)$ observations of lag distance h_i, and $\Gamma(h_i)$ denote the experimental semivariogram value at lag h_i ($i = 1, 2, \ldots n$). Using the spherical model of experimental semivariogram expressed in Eq. (4), we can substitute the experimental values into the transformed linear Eq. (5) as follows:

$$\begin{aligned} &a_{11}x_1 + a_{12}x_2 + a_{13}x_3 = b_1 && \text{when lag} = h_1 \\ &a_{21}x_1 + a_{22}x_2 + a_{23}x_3 = b_2 && \text{when lag} = h_2 \\ &\cdots && \cdots \\ &a_{n1}x_1 + a_{n2}x_2 + a_{n3}x_3 = b_n && \text{when Lag} = h_n \end{aligned} \quad (6)$$

where (b_1, b_2,...b_n) are all greater than zero. Eq. (6) can be written in matrix form as:

$$\mathbf{Ax} = \mathbf{b} \tag{7}$$

where:

$$\mathbf{A} = \begin{bmatrix} a_{11} & a_{12} & a_{13} \\ a_{21} & a_{22} & a_{23} \\ \cdots & & \\ a_{n1} & a_{n2} & a_{n3} \end{bmatrix}, \mathbf{x} = \begin{bmatrix} x_1 \\ x_2 \\ x_3 \end{bmatrix}, \mathbf{b} = \begin{bmatrix} b_1 \\ b_2 \\ \cdots \\ b_n \end{bmatrix} \tag{8}$$

To find a nonnegative solution of Eq. (6) (to ensure a nonnegative variance), the constraint $\mathbf{x} \geq \boldsymbol{\theta}$ has to be considered, where $\boldsymbol{\theta}$ is a vector of which all components are zero. Using an objective function for $\mathbf{x}$ that includes this constraint, and minimizing the function through linear programming techniques with the experimental semivariance data for h_i, would produce a new vector:

$$\mathbf{x}^0 = [x_1^0,\ x_2^0,\ x_3^0]^{\mathrm{T}} \tag{9}$$

which is the solution of the linear Eq. (6). The superscript T in Eq. (9) stands for transpose. The model parameters a and c can be determined from this solution and the fitted semivariogram can be plotted using these parameters. Chen and Jiao (2000) have provided a detailed discussion of the procedure and also the required computer code for the numerical solution. For our study, we used this linear method to determine the sill and range parameters to fit the desired spherical semivariograms.

3. Data collection and processing

3.1. Sampling methods

This study was conducted in selected chaparral and grassland vegetation sites in the Santa Monica Mountains region of southern California (Fig. 2). Data were collected during the Fall seasons of 1998 and 1999 and the Spring of 2000, using a combination of field sampling and AVIRIS imagery (Table 1). Our intention was to obtain field- and aircraft-based hyperspectral data in different seasons when water availability and physiological activity of the vegetation varies greatly. Due to the Mediterranean climate, Fall is the dry season in southern California and greening occurs in winter and Spring following winter rains. Chaparral sites were also selected based on fire history and included locations that had burned 1, 3, 21 and over 40 years ago. These age classes corresponded to striking differences in cover and vegetation structure resulting from post-fire succession. Since most southern California grassland species are annuals, this vegetation type undergoes less structural change than chaparral over comparable time periods. Hence, only two grassland sites were selected for this study: one in the Fall of 1998, and another during the Fall of 1999 and the Spring of 2000. These grassland sites were located near each other in a locality named Rancho Sierra Vista. The grassland site selected for study in 1998 had been burned 5 years earlier, and the other site had been burned 6 months prior to measurement.

Field sampling was conducted along the selected transects in each test site with a field spectrometer (UniSpec, PP Systems, Haverhill, MA) fitted with a straight fiber foreoptic. The end of this fiber optic, which was positioned 3 m above the ground, yielded a field-of-view of approximately 20°, resulting in a "pixel size" of approximately 1 m on the ground. This spectrometer collects data at wavelengths from 300 to 1100 nm at approximately 3-nm intervals and in band widths (full width at half maximum) of 10 nm, with a controllable scanning time to allow optimal exposure based on incoming light level. It has 256 spectral bands and the data were saved in digital format for subsequent processing. By scanning at 1-m intervals while walking along premarked 100-m transects at each site, we obtained 100 ground spectra of approximately 1-m-diameter contiguous pixels. Sunny days were chosen for field trips and data collection time was bracketed between 2 h before to 2 h after solar noon. Each transect was completed within half an hour to ensure that the solar zenith did not change significantly from beginning to end of the transect.

A 99% reflective white reference (Spectralon, Labsphere, North Sutton, NH) was placed on a level tripod in an open sunny area near the transects. Before every 20–25 ground measurements, we scanned the reference with the spectrometer to collect the reference radiance (i.e., solar irradiance). Dividing the spectral radiance of the target by the reference radiance produced the surface reflectance. We also used a linear interpolation technique to interpolate the original 3-nm spectrometric data to an interval of 1 nm. Since the digital signals prior to 400 nm and after 1000 nm were noisy, our final surface reflectance data consisted of 400–1000 nm, at an interval of 1 nm, i.e., a total of 601 spectral bands.

In the Fall of 1998, hyperspectral data were collected from one chaparral transect and one grassland transect at the Rancho Sierra Vista site simultaneously with a low-altitude AVIRIS flight (on 5 October) covering the same area. Low-altitude AVIRIS flies at approximately 5000 m above the ground and yields a pixel size of approximately 4 m. We corrected the AVIRIS image for atmospheric scattering and absorption using the atmospheric correction program ATREM (Reference: University of Colorado, Boulder, web page: http://cires.colorado.edu/cses/atrem.html) and cut a 400 × 250-pixel subset (or 1.6 km × 1.0 km) of it covering the study region. This subset image was then georeferenced for the study purpose.

Field sampling was conducted at 10 other widely distributed chaparral sites and one grassland site (near Rancho

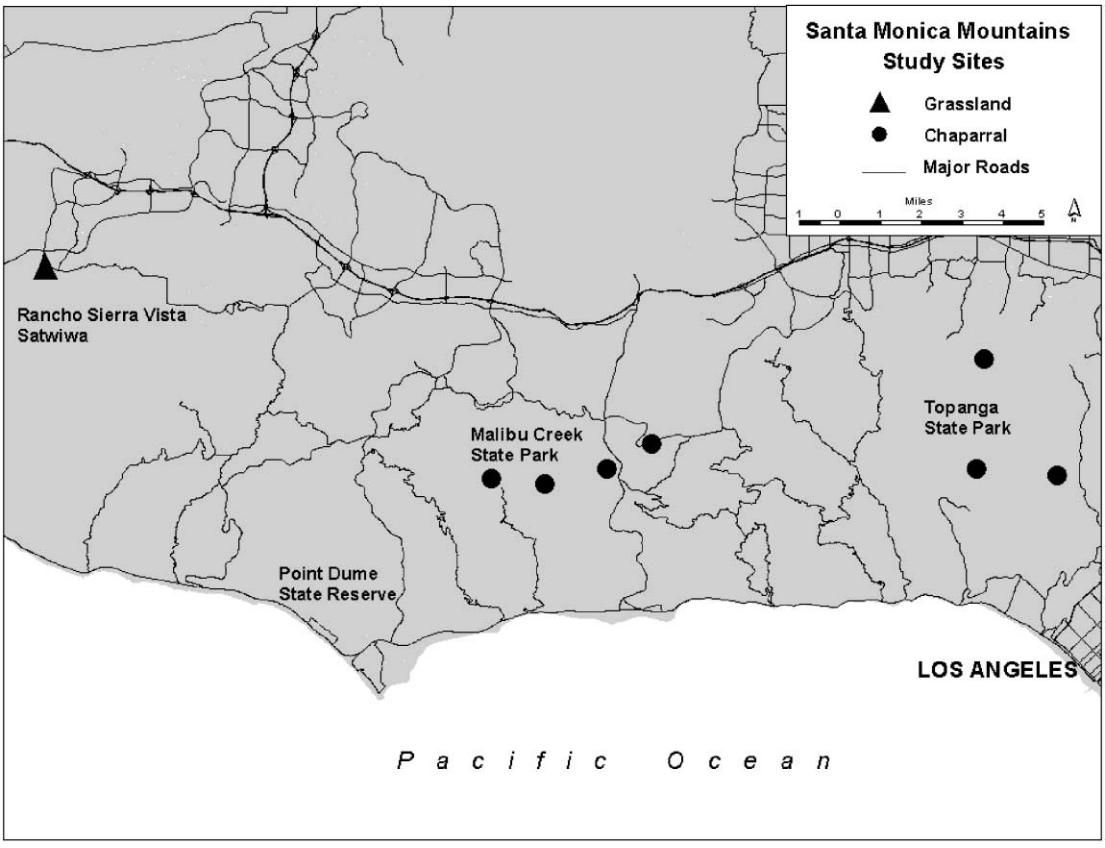

Fig. 2. A map of the study sites in the Santa Monica Mountain region of southern California. The seven areas for chaparral are shown, which contained the 10 transects. The Rancho Sierra Vista site contained the two grassland transects.

Sierra Vista) during the Fall of 1999 and the Spring of 2000. No simultaneous AVIRIS data were available for comparison with the field data from 1999 and 2000. Chaparral sites were mostly dominated by buckbrush. Other common species included chamise, wild buckwheat and laurel sumac, along with occasional patches of annuals or bare ground. The grasslands were dominated by rye grass with a mix of wild oats and wild radish. Soil background was covered by annual vegetation in the grassland sites (Table 2). During the Fall of 1998 and 1999, the grasslands were mostly brown

Table 1
List of all ground-based data sets used in this study

Date of data collection	Age	Vegetation
Fall 1998		
10/5	23 years	chaparral
10/5	1 year (senescing)	grassland
Fall 1999		
11/22, 11/24	1 year	chaparral
11/23, 12/10, 12/16	3 years	chaparral
12/10, 12/15, 12/16	21 years	chaparral
12/15, 12/16	>40 years	chaparral
12/03, 12/08	1 year (senescing)	grassland
Spring 2000		
04/24, 04/26	1 year	chaparral
04/10, 04/12, 06/20	3 years	chaparral
04/10, 04/12, 06/20	21 years	chaparral
04/24, 06/20	>40 years	chaparral
04/04, 04/11	1 year (green)	grassland

The accompanying AVIRIS image was available only for the fall of 1998 data sets.

Table 2
List of the plant scientific names present in the transects used in this study in alphabetic order

Scientific name	Common name
Adenostoma fasciculatum	chamise
Artemesia californica	coastal sagebrush
Avena fatua	wild oats
Bomus diandrus	ripgut brome
Brassica nigra	black mustard
Ceanothus cuneatus	sedge-leaf buckbrush
Ceanothus megacarpus	big-pod buckbrush
Convulvulus arvensis	field bindweed
Eriogonum fasciculatum	california wild buckwheat
Lolium muliflorum	rye grass
Lotus scoparius	western bird's-foot-trefoil
Lupinus truncates	collared annual lupine
Malacothamnus fasciculatus	mendocino bush-mallow
Malosma laurina	laurel sumac
Phacelia cicutaria	caterpillar scorpion-weed
Raphanus raphanistrum	wild radish
Salvia mellifera	black sage

with some green patches, and the chaparral species were green but stressed following summer drought. In the Spring of 2000, grassland and chaparral species were lush green.

All of our transects were selected so that they were at a similar climatic region and at a similar distance from the Pacific Ocean (Fig. 2). No specific geographic direction (north–south, or east–west, etc.) was followed in setting up the transects. Aspects of the transects ranged from south to west, elevation ranged from 700 to 2000 m, and distances from the coast were 8–16 km. The sites were selected to be as similar to each other as possible except for stand age. This way we could ignore the directional bias and render an isotropic characteristic to our transect data. All transects were 100 m long and were relatively accessible from roads or trails.

3.2. Hyperspectral indices NDVI, PRI and WBI

The Normalized Difference Vegetation Index (NDVI) is an expression of contrasting reflectance between red and near-infrared regions of a surface spectrum (Rouse, Haas, Schell, Deering, & Harlan, 1974). This expression is a readily usable value that can be directly related to green vegetation cover or measure of vegetation abundance, and is expressed as:

$$\mathrm{NDVI} = \frac{R_{\mathrm{NIR}} - R_{\mathrm{RED}}}{R_{\mathrm{NIR}} + R_{\mathrm{RED}}} \tag{10}$$

where R_{NIR} is near-infrared (NIR) reflectance, and R_{RED} is the red reflectance.

This index is sensitive to the presence of green vegetation (Sellers, 1985), and has been found well correlated with biomass and green leaf area index in chaparral and grassland of California (Gamon et al., 1995). It has been used for numerous regional and global applications for studying the distribution and potential photosynthetic activity of vegetation (Deblonde & Cihlar, 1993; Myneni, Los, & Asrar, 1995; Prince & Tucker, 1986; Townshend & Justice, 1986; Tucker, Fung, Keeling, & Gammon, 1986, among others). Since the formulation of NDVI permits a normalization of red/NIR ratio, it acts as a robust descriptor of green vegetation in spite of varying atmospheric effects in the red and NIR bands (Fraser & Kaufman, 1985; Holben, Kaufman, & Kendall, 1990; Kaufman, 1984). We used reflectance values at a wavelength of 680 nm as red and 800 nm as NIR (Fig. 3).

Hyperspectral reflectance can also be used to monitor the activity of xanthophyll cycle pigments (Gamon et al., 1990). One spectral index used for this purpose is the Photochemical Reflectance Index (PRI), expressed as:

$$\mathrm{PRI} = \frac{R_{531} - R_{\mathrm{REF}}}{R_{531} + R_{\mathrm{REF}}} \tag{11}$$

where R_{531} represents reflectance at 531 nm (the xanthophyll cycle wavelength) and R_{REF} indicates reflectance at a reference wavelength (Gamon, Serrano, & Surfus, 1997; Peñuelas et al., 1995). The reference wavelength used for the present study was 570 nm (Fig. 3). Previous studies have shown that the use of 570 nm as the reference wavelength reduces the effect of changes in reflectance produced by chloroplasts (Méthy, 2000; Peñuelas et al., 1995). Since xanthophyll cycle pigments regulate photosynthetic light use (Demmig-Adams & Adams, 1996; Pfündel & Bilger, 1994), and interconversions of these pigments are detectable with spectral reflectance (Gamon et al., 1990), PRI provides a measure of radiation use efficiency of vegetation (Fillela et al., 1996; Gamon, Peñuelas, & Field, 1992; Gamon et al., 1997; Peñuelas et al., 1995; Rahman, Gamon, Fuentes, Roberts, & Prentiss, 2001).

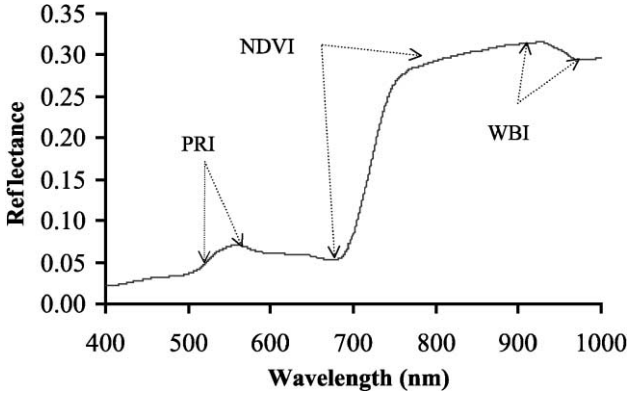

Fig. 3. Diagram showing the spectral regions for computing the three indices used in this study, namely, Normalized Difference Vegetation Index (NDVI), Photochemical Reflectance Index (PRI) and Water Band Index (WBI).

At 970 nm, there is a trough in the reflectance spectrum of green vegetation due to water absorption. This trough tends to disappear from the reflectance spectra of water-stressed vegetation as canopy water content declines (Peñuelas et al., 1997). A canopy water status index (termed Water Band Index, or WBI) has been defined as a ratio of reflectance at 970 nm and at a reference reflectance, such as 900 nm, and is defined as:

$$\mathrm{WBI} = \frac{R_{970}}{R_{900}} \tag{12}$$

where R is the reflectance (Fig. 3). The reflectance at 900 nm is used as reference because there is no absorption by water at this wavelength, but it is subjected to the same changes in structure as the reflectance at 970 nm. This water index has been found to be highly correlated with plant water content in several species of trees, shrubs, crops and grasses (Peñuelas et al., 1997).

3.3. Spatial analysis

For all three seasons, NDVI, PRI and WBI of each transect point were calculated using Eqs. (10), (11) and (12), respectively. Additionally, we also produced images

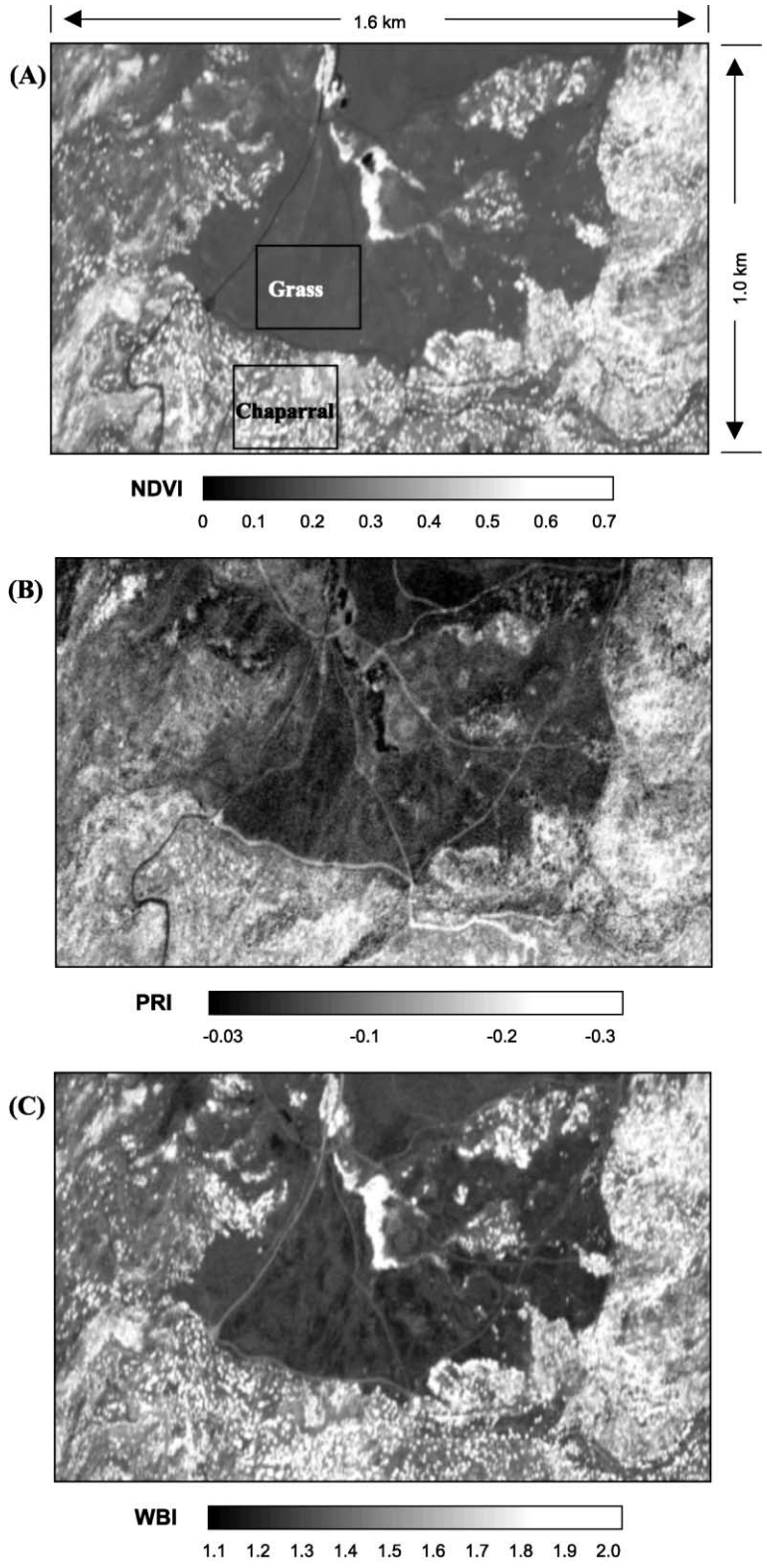

Fig. 4. Low-altitude AVIRIS Indices scene (400 × 250 pixels, or 1.6 × 1.0 km), dated 5 October 1998 from the Rancho Sierra Vista site in the Santa Monica Mountains, CA (34°8′ 32″ N, 118°57′ 19″ W). Note the similar landscape patterns for NDVI (A) and WBI (C), suggesting that most of the water detectable in this image was present in green leaves. PRI (B) had different spatial patterns than both NDVI and WBI, indicating that it senses different aspects of green vegetation than NDVI and WBI. Also indicated in (A) are the chaparral and grassland areas (50 × 50 pixels) used for the average local variance estimates in this study. In this low-altitude image (pixel size approximately 4 × 4 m), bright spots indicate individual canopies or small patches of relatively uniform shrub or tree cover, generally not resolvable in high-altitude scenes.

of these indices from the 1998 AVIRIS image (Fig. 4). AVIRIS band #30 was used for red reflectance and band #47 was used for NIR reflectance. PRI was calculated using bands #17 and #21 for 531 and 570 nm wavelengths, respectively. For calculating WBI, bands #57 and #65 were used to provide wavelengths at 900 and 970 nm, respectively.

Experimental semivariograms were calculated using these vegetation index data from all the ground-based transects. When constructing the semivariograms, we had to choose a maximum number of lags to include in the model fitting. Since the length of lags determines the number of those lags in a given transect, the longer the lag, the fewer is their number. As a result, the confidence that can be ascribed to a semivariance $\Gamma(h)$ decreases with increasing lag distance h (Curran, 1988). It is inadvisable to interpret lags longer than a fifth to a third of the transect length because of insufficient sample size (Webster, 1985). In this study, we used lags up to a fifth of the transect length, i.e., 20 m, for all subsequent analyses.

Since our goal was to find an optimal pixel size for the large, heterogeneous areas of the Santa Monica Mountains region rather than for each individual transect, we resorted to an averaging procedure for the semivariance data. This was done by the use of a pooled point-support variogram across all transects. The effect is similar to that of aggregation, and it reduces the overall high frequency variations in the variance (Woodcock, Strahler, & Jupp, 1988).

For chaparral, we first calculated the semivariance of each transect for lags up to 20 m. Then, for each lag h_i ($i=1, 2,\ldots 20$), we averaged the semivariance for that lag from all transects for one season. These average semivariances were then considered as representative values for all of the chaparral transects, and hence, for the chaparral vegetation of the study region for that season. Similarly, we produced point-support semivariance values for grassland. This averaging scheme is expressed mathematically as follows:

$$\overline{\Gamma(h_i)} = \frac{1}{k}\sum_{j=1}^{k}\Gamma(h_i)_j \tag{13}$$

where $i=1, 2,\ldots 20$, $k=10$ for chaparral and 3 for grassland in both 1999 and 2000. Since the1998 chaparral and grassland data were from only one transect each, no averaging was done for those data sets. All of these semivariance data sets were then used for spherical semivariogram model fitting by utilizing the linear programming methods described in Eqs. (6)–(9).

As a further means of examining the optimal pixel size, we used the Average Local Variance (ALV) procedure with the 1998 AVIRIS image. ALV is defined as the average value of the variance within a 3×3 moving window passing through any selected part of an image (Woodcock & Strahler, 1987). For example, if the selected part of the image has L rows by M columns and a pixel size v, then the ALV of that image subset can be estimated by (Curran & Atkinson, 1999):

$$\sigma_v^2 = \frac{1}{L\times M}\sum_{l=1}^{L}\sum_{m=1}^{M}\frac{1}{9}\sum_{j=-1}^{+1}\sum_{k=-1}^{+1} \times\left[\overline{z_v}(l+j,m+k)-z_v(l+j,m+k)\right]^2 \tag{14}$$

where σ_v^2 is the ALV, $\overline{z_v}$ is the average of the moving 3×3 window surrounding a center pixel z_v, and j and k are two counters for that window.

ALV is calculated for a range of integer multiples of the original pixel size v and expressed as a function of pixel size. The spatial resolution at which the peak occurs may help to identify the optimal pixel size for studying surface processes. The rationale behind this technique is that, at a

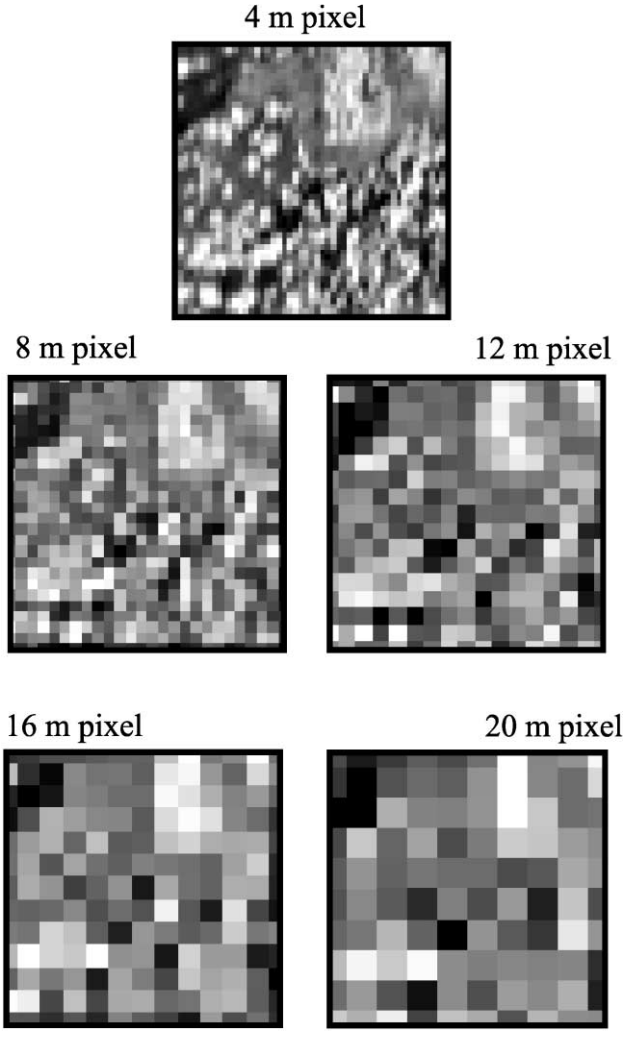

Fig. 5. An example of the integer multiple of original 4-m pixels that were used for the average local variance (ALV) estimation. Here, a subregion of the chaparral NDVI image is shown at 4-, 8-, 12-, 16- and 20-m pixel resolutions. The original 4-m pixels were degraded to the larger pixels and then the ALV was calculated from each of these images using a 3×3 moving window.

high spatial resolution where the pixel sizes are smaller than the surface structures, the neighboring pixels would be highly correlated and hence a low variance would exist among them. With increasing pixel size, this similarity decreases and variance increases. However, as the pixel size increases beyond the scale of spatial variation, more dissimilar surfaces would be contained in one pixel and the local variance would start decreasing. Therefore, the pixel size at which the peak ALV occurs would identify the predominant spatial variation in the image. The ALV thus obtained should be similar to the point-support variogram of the region (Vargas-Guzmán, Myers, & Warrick, 2000).

We used a 50 × 50-pixel subset from each of the grassland and chaparral areas of the 1998 AVIRIS image to examine the ALV, and hence the optimum pixel sizes, for NDVI, PRI and WBI of those two areas (Fig. 4A). This subset size was chosen in order to fit a square image window with a continuous coverage of one type of vegetation (grassland or chaparral). Also, our grassland and chaparral transects in that site fell inside these image subsets. Since the original image had a 4-m pixel size, we used 8-, 12-, 16- and 20-m pixel sizes as the integer multiples of the original pixels (Fig. 5). To produce larger pixels, we reduced the resolution of the original 4-m image by integer factors 2, 3, 4 and 5 in the X and Y directions and averaged all of the original "small" pixels to make up the new "big" pixels. Then, we used Eq. (14) with a 3×3 running window to calculate the ALV for each of these resampled images.

4. Results

4.1. Semivariogram

Semivariogram model fits using the NDVI, PRI and WBI data sets for all three seasons indicate that there was always some nugget variance present (Figs. 6–8). During the reflectance measurement of vegetated surfaces, there is always a possibility of slightly varying FOV, sun angle, sky conditions, temporally changing surface characteristic, or other sources of variability, and hence a nonzero nugget in the semivariogram. In contrast to many artificial surfaces, biological materials that can change their structure and

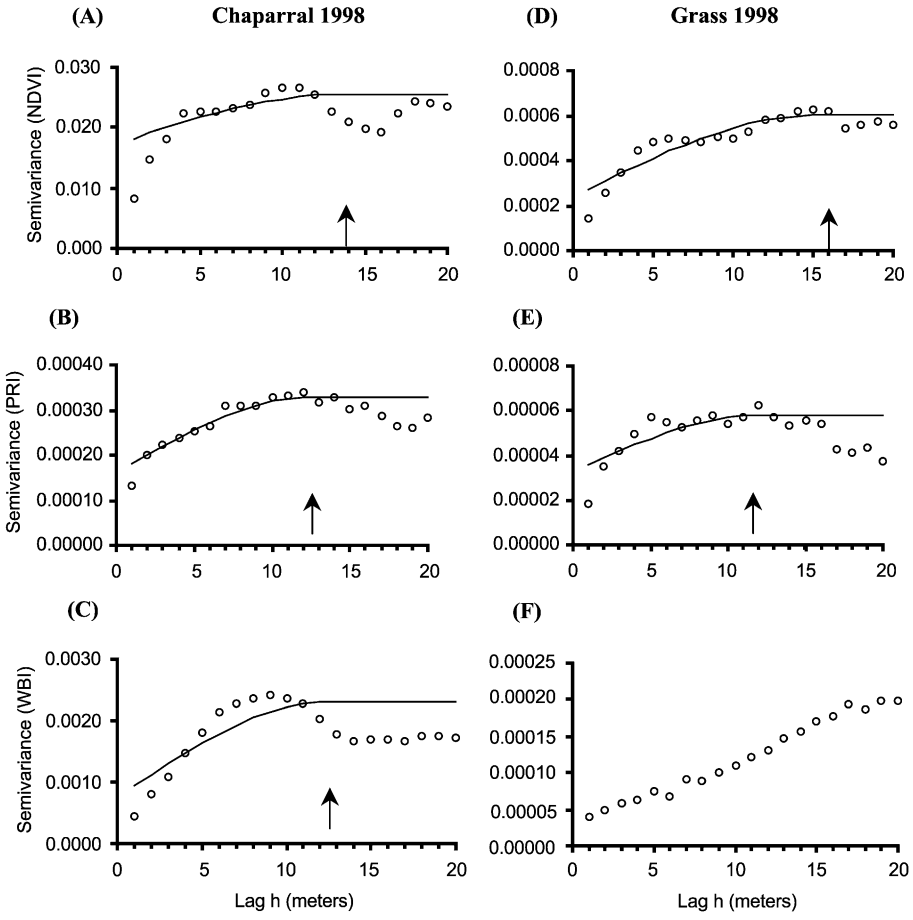

Fig. 6. Semivariograms for chaparral and grassland in the Fall of 1998, with data points shown as hollow dots and model fit as solid lines. The arrows show the ranges at which sills were attained. As mentioned in the text, only the spherical semivariogram model was fitted using the data sets. WBI semivariance (F) did not attain a sill within the 20-m lag.

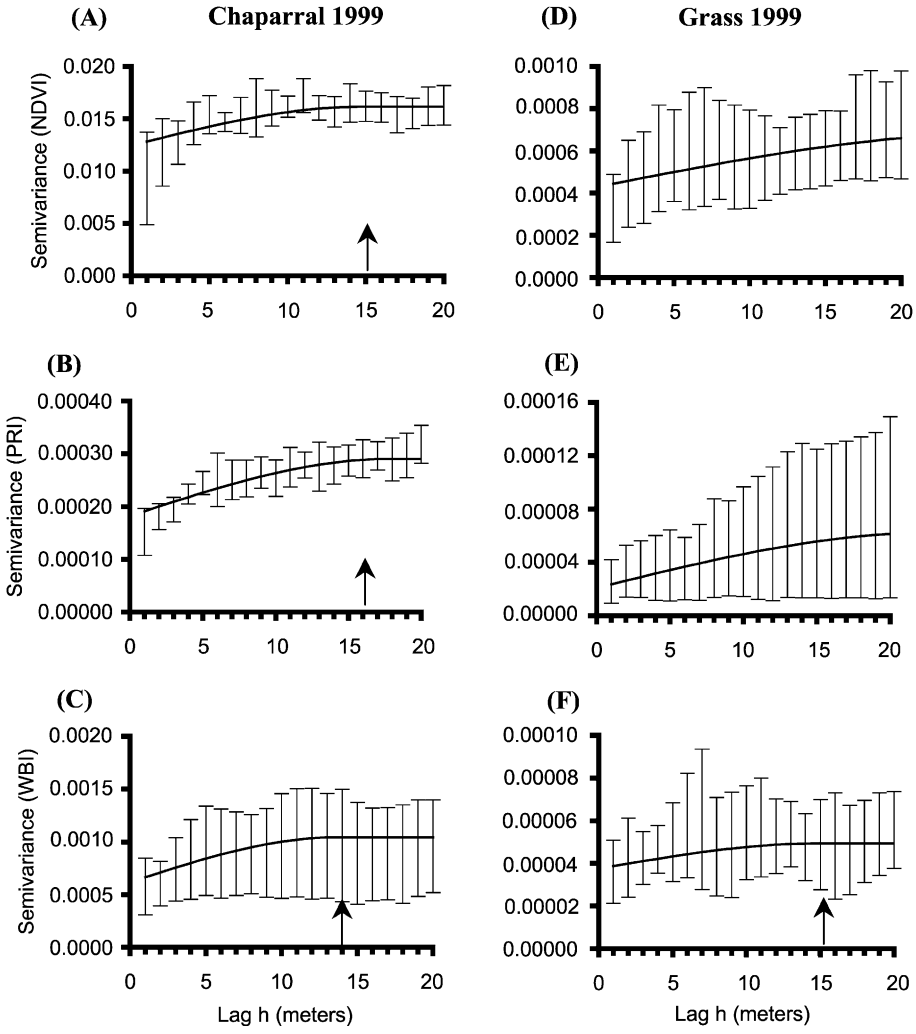

Fig. 7. Similar to Fig. 6, but with data from the Fall of 1999. The error shows the upper and lower limits of semivariance in the experimental data from different transects, and the solid lines show the model fits using the regularized variances from those experimental data. Range values are shown with arrows. Grassland NDVI (D) and PRI (E) did not attain a sill within the 20-m lag used for this study.

physiology over short time intervals (e.g. seconds to minutes) may be particularly prone to these sources of error. It can also be seen in Figs. 6–8 that the variances in chaparral transects were always higher than those in grass. However, since the reason for using the semivariogram was to determine the optimum pixel size, the characteristic of the 'range' was our main concern.

In the Fall of 1998, the range of NDVI from the chaparral transect was14 m, and those of PRI and WBI were 13 m, even though the experimental data showed a somewhat cyclic characteristic at a lag of approximately 12 m (Fig. 6A, B and C). The model fits are shown as solid lines, along with the experimental semivariance data shown as hollow dots. Grass semivariance for 1998 attained sills at ranges 16 and 12 m, respectively, for NDVI and PRI, but the model did not attain a sill for WBI data (Fig. 6F). In the latter case (grass WBI), the semivariance data showed rather a linearly increasing trend up to 18 m lag and then seem to attain a sill beyond 20 m.

In the Fall of 1999, semivariance model outputs of NDVI, PRI and WBI from chaparral transects attained sill at ranges of 15, 16 and 14 m, respectively (Fig. 7A, B and C). On the other hand, semivariance model outputs of NDVI and PRI from grassland transects failed to attain sills within the 20-m lag (Fig. 7D and E). The semivariance of WBI from grassland transects attained a sill at a 15-m range (Fig. 7F). In these figures, the error bars with crosses at the end show the upper and lower limits of semivariance in the experimental data from different transects, and the solid lines show the model fits using the regularized semivariances from those experimental data. The scatters in the semivariance of experimental data were lower for chaparral NDVI and PRI (Fig. 7A and B) than those in the other four diagrams (Fig. 7C–F). However, it is noticeable that the scatter generally followed the trend of the model fit in case of attaining a range. For grassland NDVI and PRI in 1999 (Fig. 7D and E), where the model could not attain a range within 20 m,

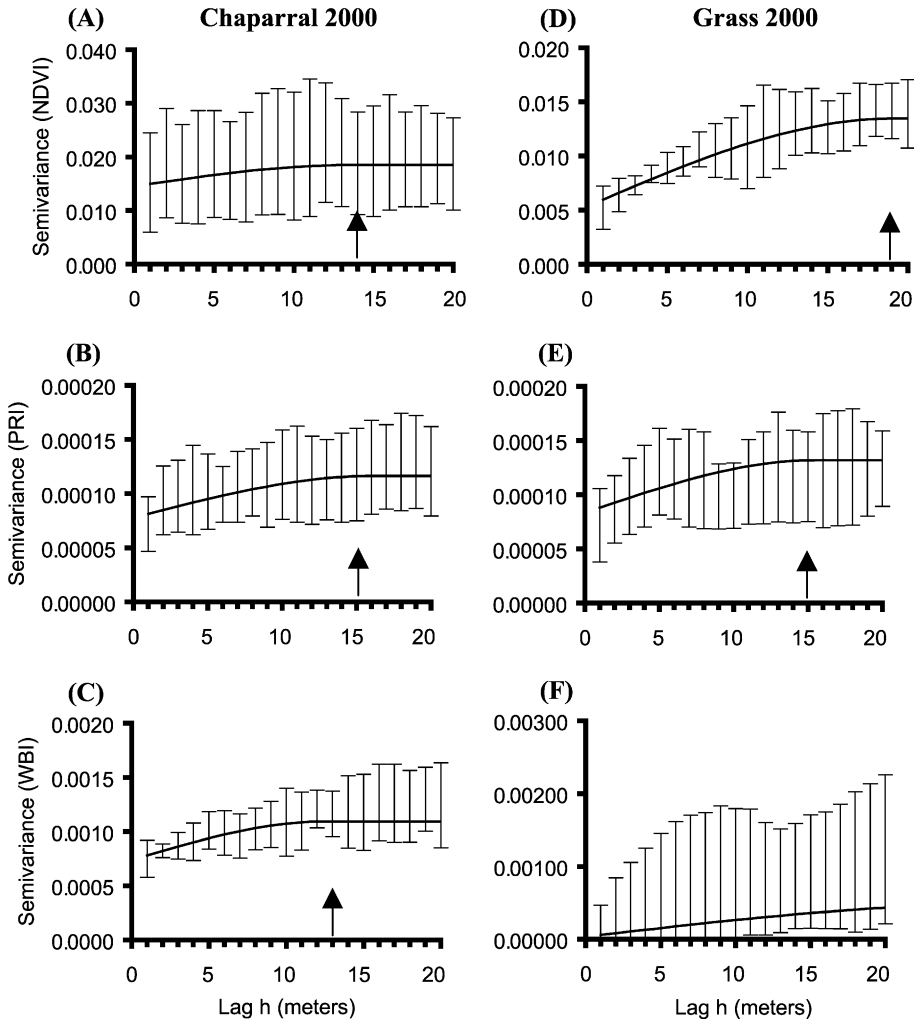

Fig. 8. Semivariograms for chaparral and grassland data collected in the spring of 2000. Here again, grass WBI did not attain a sill within the 20-m lag. Error bars, solid lines and arrows represent information similar to that in Fig. 7.

the semivariance of field data also showed a linearly increasing tendency, rather than attaining a sill. Since the point-support semivariances were used to fit the semivariogram model, this agreement between data and model output was expected.

The chaparral transects in the Spring of 2000 had similar range values as those in the Fall of 1999: 14 m for NDVI, 15 m for PRI and 13 m for WBI (Fig. 8A, B and C). The scatters in the experimental variances were higher in chaparral NDVI and PRI than those in 1999, but the scatter in WBI experimental semivariances was lower. The Spring grassland transects had higher range values, similar to those in Fall of previous years. The range for grassland NDVI was 19 m, and for PRI, it was 15 m (Fig. 8D and E). Once again, the WBI could not attain a sill within the 20-m lag, hence, the range was greater than 20 m (Fig. 8F). A summary of all range values is given in Table 3. For all three indices discussed in this paper for the three seasons, chaparral ranges varied from 13 to 16 m, and grassland ranges varied from 12 to 19 m, exceeding 20 m in a few cases, and not fitting a semivariogram model in one case. It is noticeable that all chaparral indices always had a range within the 20-m lag, whereas the grassland indices were the ones with ranges outside 20 m.

Table 3
Semivariogram ranges calculated from the transects of hyperspectral indices of chaparral and grass in all three seasons

Season	Index	NDVI	PRI	WBI
Fall 1998	chaparral	14	13	13
	grassland	16	12	>20
Fall 1999	chaparral	15	16	14
	grassland	>20	>20	15
Spring 2000	chaparral	14	15	13
	grassland	19	15	>20

The unit is meters (m). The range is expressed as >20 when a sill was not attained within the 20-m lag.

4.2. Local variance

The ALV method was tested using the AVIRIS image data from the Fall of 1998. All indices showed a marked increase in ALV as the pixel size increased from 4 to 8 to 12 m, and attaining peaks at 16 m, except for chaparral PRI, which peaked at 12 m (Fig. 9A, B and C). Beyond the peak, the ALV again decreased. These results indicated that the local variance for both grassland and chaparral sharply decreased when the aggregation of pixels exceeded 16 m (12 m for chaparral PRI).

Similar to the semivariogram analysis, the values of chaparral variances at each pixel size for all three indices were always higher than those for grassland. A visual observation of the ALV graphs (Fig. 9) shows that except for chaparral PRI, the rate of decrease of all other ALV values from the peak to the 20-m pixel size was steeper than their rate of rise from 4 m to the peak, indicating a rapid decrease in spatial variance as the pixel size increases to 20 m.

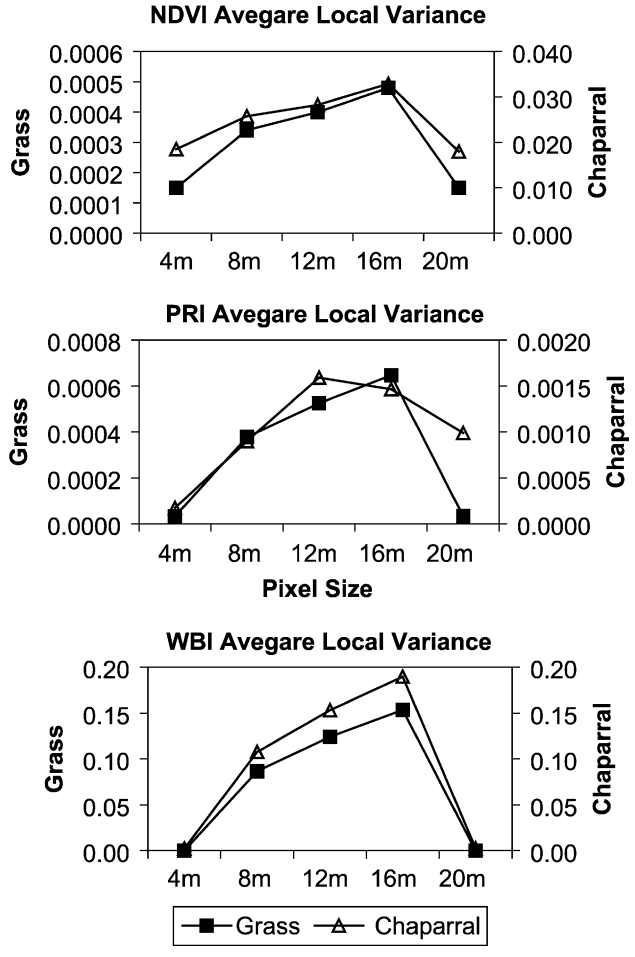

Fig. 9. Average local variance of the 50 × 50-pixel subset of chaparral and grass indices, calculated from the 1998 AVIRIS image. Except for the chaparral PRI, all other ALVs peaked at 16 m and then decreased. The chaparral ALV peaked at 12 m.

5. Discussion

The semivariograms from all transects using all three hyperspectral indices (NDVI, PRI, WBI) showed that for the chaparral and grasslands, 12 m was the lowest range (Table 3). Since we are concerned about the limit at which spatial variance may begin to decrease due to aggregation, we chose the lowest limit among the ranges. Following the sampling theorem (McGrew & Monroe, 2000), this indicates that a pixel size larger than 6 m may lose spatial information due to averaging. On the other hand, a much smaller pixel size than this 6-m range would mean an unnecessarily large volume of data. Hence, a balance is needed in the choice of an optimum pixel size.

The ALV results of Rancho Sierra Vista chaparral and grass images closely matched the results obtained from the semivariogram analysis. Local variances peaked at pixel size of 16 m, with the exception of chaparral PRI, which attained peak at 12 m. These results indicate that 6 m (half of the lowest among the ALVs) would be the optimum pixel size for studying these hyperspectral indices, which is very similar to the results obtained from the semivariance studies.

Since the ALV were calculated using only one site of chaparral and grassland at Rancho Sierra Vista, these results by themselves may not have been as widely applicable as the semivariogram analysis that was done using data from a wide range of sites. However, the similarity of ALV results with the semivariogram analysis provide confidence that 6 m may be safely considered a suitable pixel size for ecosystem studies in the Santa Monica Mountains using hyperspectral remote sensing.

Chaparral vegetation of Santa Monica Mountains region has a readily visible structural pattern, with clumps of shrubs and occasional open patches, which in turn may be partially covered by grasses or forbs. For chaparral, the range of approximately 12 m appears to correspond roughly with the scale of these visible patterns. Grassland, on the other hand, generally appears more homogenous, even though at fine scales (<1 m) multiple patches and species may be present. For grassland, the lack of a clear range between 1 and 20 m fits the lack of clearly visible patterns at the 1–20-m scale. These contrasting structures of these two vegetation types can be easily recognized from photographs of these areas (Fig. 10).

A visual analysis in the field suggested that the sampling distance of 6 m obtained from this study corresponded roughly with the half of the size of patches of functionally similar vegetation (e.g. patches dominated by a single group of species or functional type such as evergreen or drought-deciduous vegetation). Given that the analyses were based on indices with well-understood structural and physiological relevance (i.e., green leaf area index, photosynthetic activity and water content), it is reasonable to conclude that the 6-m sampling distance emerging from these analyses represents a fundamental scale for analyzing certain key ecosystem processes at local and regional scales. For example, land-

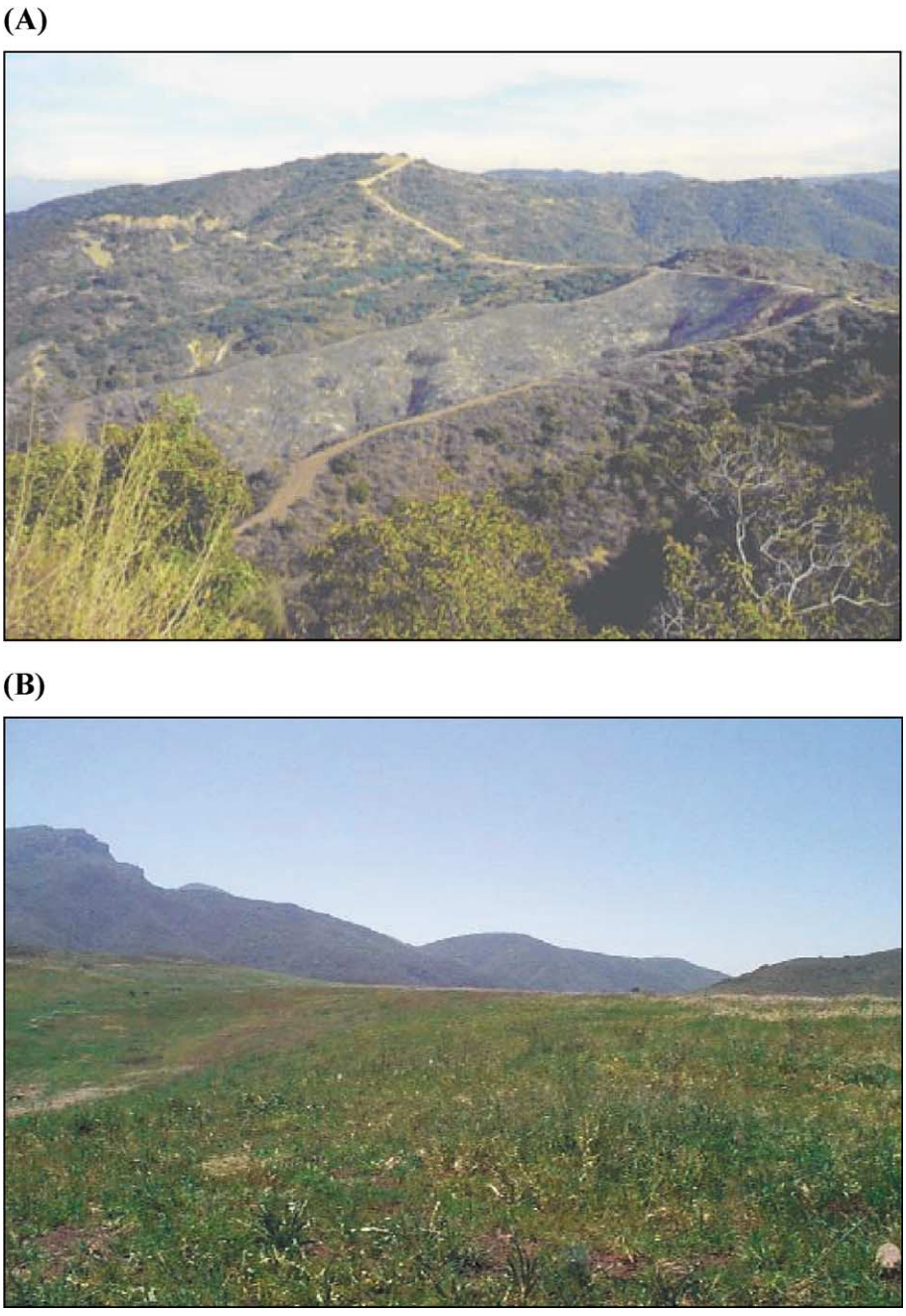

Fig. 10. Photograph of a representative chaparral site (A) and a grassland site (B). The chaparral site has a recently burned region visible in the middle, with 3-year-old stands in the unburned areas. The patchiness of the landscape (associated with shrub clusters and bare regions) is clearly visible from this picture. Grassland typically appears more uniform, with some visible variation due to gradients in productivity (e.g. associated with terrain and varying soil moisture). Note that very fine scale (<1 m) patterns are present, but not resolvable with the methods used here.

scape patterns of leaf area index (LAI), biomass, photosynthetic flux and evapotranspiration of vegetation in the study region can probably be well described using this fundamental pixel size.

This 6-m fundamental scale emerging from this study is slightly smaller than that emerging from a previous analysis of one northern California grassland using AVIRIS high-altitude imagery (Gamon, Field, Roberts, Ustin, & Valentini, 1993). That study concluded that a pixel size of roughly18–20 m (equivalent to high-altitude AVIRIS pixel size) adequately captured variations in grassland greenness and photosynthetic activity associated with larger patterns of slope, aspect and soil type, but missed finer scale variability associated with individual plants. Unlike our study, that previous study did not conduct independent field sampling at the sub-18-m scale and lacked the low-altitude AVIRIS imagery that has only recently become available on a limited basis. Also, the results of our analyses showed that

in several cases, a 20-m pixel size could have been suitable for studying the more visibly homogenous grassland but not suitable for the chaparral areas.

Thus, one conclusion from this analysis is that the selection of the "ecologically fundamental scale" is, to some extent, determined by the range of pixel sizes used in the analysis. Many current satellite and aircraft sensors (e.g. TM with its 30-m pixel size, or AVHRR with its 1.1-km pixel size) simply cannot resolve finer scales, and thus would not be able to detect potentially important patterns below these scales. Similarly, because 1 m was the fundamental inter-sample distance (i.e., lag) used in our study, we necessarily ignored potentially important spatial patterns at much finer scales. For example, sub-meter patterns of seed germination and subsequent seedling survival commonly studied in ecological plot studies are undoubtedly relevant to larger ecosystem processes, particularly in the early regeneration stages after a fire. However, the 1-m scale was more than adequate to capture larger scale patterns associated with assemblages of similar vegetation type.

Researchers have previously shown that the canopy physiological processes (such as CO_2 and water fluxes) and structural characteristics (such as biomass and leaf area index) can be studied using remote sensing. Recent advances in hyperspectral remote sensing indicate that the narrow band indices can track specific physiological signals (such as photosynthetic pigments) more efficiently than the broad-band indices. Based on these promising results, NASA is planning to launch hyperspectral imager satellites in the near future (for details see http://nmp.jpl.nasa.gov). For efficient use of these hyperspectral images, ecosystem scientists need to specify the suitable spatial scales for data collection. Our study is a step forward toward that direction, showing the optimal spatial scale for mapping biomass, photosynthetic flux and water content of a semiarid biome in southern California.

6. Error statements and future directions

The results obtained in this study are based on sound geospatial techniques, but these were not exhaustive. Rather, these results have answered some questions and raised some new concerns, which are discussed next. Both the semivariogram and ALV approaches have some associated errors that should not be overlooked in interpreting the results obtained in this study. For semivariogram analysis, theoretical model fitting using experimental data may introduce error (Oliver, 1996). Also, the calculation of point-support semivariance (Eq. (13)) might have compromised some of the variances and hence the outcome of the range values, even though this scheme helped in avoiding the transect-specific semivariograms and provided regional generality to the results.

Another issue not addressed in this study is the inclusion of terrain and substrate, and their potential influence on the hyperspectral signatures and ultimately on the spatial characteristics of vegetation function. However, the relatively level terrain minimized these concerns at our sites, but may be more important at other locations. These issues are the subjects of our continuing research.

7. Conclusions

The main purpose of the analyses presented in this paper was to investigate the effects of spatial scale on hyperspectral studies of southern California ecosystem function (namely, biomass, photosynthesis and water content), and to recommend suitable pixel sizes for that purpose. Geostatistical methods of semivariogram analysis and local variance estimation were used with ground-based transect data and airborne image data, respectively. Our ground-based transects were distributed across a wide area and included chaparral vegetation of different age groups and annual grassland, representative of a large portion of the Santa Monica Mountains region and southern California vegetation in general.

Semivariogram analysis of three indices determined from the ground transects revealed that 6 m would be a pixel size that would retain most of the characteristic spatial variation of chaparral and grassland ecosystem function, which can be sensed with hyperspectral sampling. Local variance estimates using the low-flying AVIRIS image also indicated that 6 m would comprise an optimum pixel size. Because the ground-based hyperspectral signatures and the AVIRIS image were independently collected and consisted of data sets from a wide range of natural areas from three seasons of 3 separate years, this good match provided confidence in the results presented in this study.

One of the implications of these findings for the existing hyperspectral sensors such as AVIRIS is that, for ecosystem function studies of southern California vegetation, the higher resolution images acquired with low-altitude aircraft would be a better choice than the 20-m pixels acquired with high-altitude flights. For designing future airborne and satellite-based hyperspectral sensors, these results may provide a guideline for selecting their spatial resolutions.

Acknowledgements

We extend our appreciation to the staff at the National Park Service who provided access to the field site, to Rob Green and the rest of the AVIRIS team for supplying a low-altitude image of our field site, and to the Center for Environmental Analysis (CEA-CREST) and the Center for Spatial Analysis and Remote Sensing (CSARS) at Cal State LA for logistical support. Thanks also to the students of Biology 454-LP (Methods and Instrumentation in Environmental Science) for their assistance in the field. We greatly appreciate the comments of three anonymous reviewers.

This work was supported by grants from NASA and NSF to J. Gamon.

References

Chen, Y., & Jiao, X. (2000). Semivariogram fitting with linear programming. *Computers and Geosciences*, *27*(2001), 71–76.

Cohen, W. B., Spies, T. A., & Bradshaw, G. A. (1990). Semivariograms of digital imagery for analysis of conifer canopy structure. *Remote Sensing of Environment*, *34*, 167–178.

Curran, P. J. (1988). The semivariogram in remote sensing: an introduction. *Remote Sensing of Environment*, *24*, 493–507.

Curran, P. J., & Atkinson, P. M. (1999). Issues of scale and optimal pixel size. In A. Stein, F. Meer, & B. Gorte (Eds.), *Spatial statistics in remote sensing* (pp. 115–133). Dordrecht, The Netherlands: Kluwer Academic Publishing.

Curran, P. J., & Guyot, G. (1997). Applications/optical domain. In G. Guyot, & T. Phulpin (Eds.), *Physical measurements and signatures in remote sensing* (pp. 893–894). Rotterdam: Balkema.

Deblonde, G., & Cihlar, J. (1993). A multiyear analysis of the relationship between surface environmental variables and NDVI over the Canadian landmass. *Remote Sensing Reviews*, *7*, 151–177.

Demmig-Adams, B., & Adams, W. (1996). The role of xanthophyll cycle carotenoids in the protection of photosynthesis. *Trends in Plant Science*, *1*, 21–26.

Fillela, I., Amaro, J. L., & Peñuelas, J. (1996). Relationship between photosynthetic radiation-use efficiency of barley canopies and the photochemical reflectance index. *Physiologia Plantarum*, *96*, 211–216.

Fraser, R. S., & Kaufman, Y. J. (1985). The relative importance of scattering and absorption in remote sensing. *IEEE Transactions on Geoscience and Remote Sensing*, *23*, 625–633.

Gamon, J. A., Field, C. B., Bilger, W., Bjorkman, O., Freeden, A., & Peñuelas, J. (1990). Remote sensing of the xanthophyll cycle and chlorophyll florescence in sunflower leaves and canopies. *Oecologia*, *85,* 1–7.

Gamon, J. A., Field, C. B., Roberts, D. A., Ustin, S. L., & Valentini, R. (1993). Functional patterns in an annual grassland during an AVIRIS overflight. *Remote Sensing of Environment*, *44*, 1–15.

Gamon, J. A., Green, R. O., Roberts, D. A., & Serrano, L. (1995, August 28–30). Deriving photosynthetic function from calibrated imaging spectrometry. In G. Guyot (Ed.), *Photosynthesis and remote sensing* (pp. 55–60). France: Montpellier.

Gamon, J. A., Lee, L.-F., Qiu, H.-L., Davis, S., Roberts, D. A., & Ustin, S. L. (1998). A multi-scale sampling strategy for detecting physiologically significant signals in AVIRIS imagery. Summaries of the Seventh Annual JPL Earth Science Workshop, January 12–16, 1998. Pasadena, CA, vol. 1. (pp. 111–120) (http://makalu.jpl.nasa.gov/docs/workshops/98_docs/toc.htm).

Gamon, J. A., Peñuelas, J., & Field, C. B. (1992). A narrow waveband spectral index that tracks diurnal changes in photosynthetic efficiency. *Remote Sensing of Environment*, *4*, 35–44.

Gamon, J. A., & Qiu, H.-L. (1999). Ecological applications of remote sensing at multiple scales. In F. I. Pugnaire, & F. Valladares (Eds.), *Handbook of functional plant ecology* (pp. 805–845). New York: Marcel Dekker.

Gamon, J. A., Serrano, L., & Surfus, J. S. (1997). The photochemical reflectance index: an optical indicator of photosynthetic radiation use efficiency across species, functional types, and nutrient levels. *Oecologia*, *112*, 492–501.

Goward, S. N., & Huemmrich, K. F. (1992). Vegetation canopy PAR absorbance and the normalized difference vegetation index: an assessment using the SAIL model. *Remote Sensing of Environment*, *39*, 119–140.

Green, R. O., Sarture, C. M., Chrien, T. G., Aronsson, M., Chippendale, B. J., Faust, J. A., Pavri, B. E., Chovit, C. J., Solis, M., Olah, M. R., & Williams, O. (1998). Imaging spectroscopy and the Airborne Visible/Imaging Spectroradiometer (AVIRIS). *Remote Sensing of Environment*, *65*, 227–248.

Hari, P., Nilson, T., Salminen, R., Kaipiainen, L., Korpilahti, E., & Ross, J. (1984). Nonlinear dependence of photosynthetic rate on irradiance and its consequences for the estimates of the amount of saccharides formed. *Photosynthetica*, *18*, 28–33.

Holben, B. N., Kaufman, Y. J., & Kendall, J. D. (1990). NOAA-11 AVHRR visible and near-IR inflight calibration. *International Journal of Remote Sensing*, *11*(8), 1511–1519.

Jarvis, P. G. (1995). Scaling processes and problems. *Plant, Cell and Environment*, *18*, 1079–1089.

Jarvis, P. G., & McNaughton, K. G. (1986). Stomatal control of transpiration: scaling up from leaf to region. *Advances in Ecological Research*, *15*, 1–49.

Kaufman, Y. J. (1984). Atmospheric effects on remote sensing of surface reflectance. *SPIE Remote Sensing*, *475*, 20–33.

Lappi, J., & Smolander, H. (1984). Integration of the hyperbolic radiation response function of photosynthesis. *Photosynthetica*, *18*, 402–410.

Matheron, G. (1971). The theory of regionalized variables and its applications. *Les cashiers du centre de mophologie mathématique, no. 5*. Fontainebleau: Centre de Géostatistique.

McBratney, A. B., & Webster, W. (1981). Spatial dependence and classification of the soil along a transect in north–east Scotland. *Geoderma*, *26*, 63–82.

McBratney, A. B., & Webster, W. (1986). Choosing functions for semivariograms of soil properties and fitting them to sampling estimates. *Journal of Soil Science*, *37*, 617–639.

McGrew, J. C., & Monroe, C. B. (2000). *An introduction to statistical problem solving in geography* (2nd ed.) (p. 110). Boston: McGraw-Hill.

Méthy, M. (2000). Analysis of photosynthetic activity at the leaf and canopy levels from reflectance measurements: a case study. *Photosynthetica*, *38*(4), 505–512.

Myneni, R. B., Los, S. O., & Asrar, G. (1995). Potential gross primary productivity of terrestrial vegetation from 1982–1990. *Geophysical Research Letters*, *22*(19), 2617–2620.

Oliver, M. A. (1996). Geostatistics, rare disease and the environment. In M. Fisher, H. Schollen, & D. Unwin (Eds.), *Spatial Analytical Perspectives on GIS (GIS Data 4)* (pp. 67–85). Bristol, PA: Taylor and Francis.

Peñuelas, J., Filella, I., Biel, C., Serrano, L., & Save, R. (1993). The reflectance at the 950–970 nm region as an indicator of plant water status. *International Journal of Remote Sensing*, *14*, 1887–1905.

Peñuelas, J., Filella, I., & Gamon, J. A. (1995). Assessment of photosynthetic radiation-use efficiency with spectral reflectance. *New Phytologist*, *131*, 291–296.

Peñuelas, J., Pinol, J., Ogaya, R., & Filella, I. (1997). Estimation of plant water concentration by the reflectance water index WI (R900/R970). *International Journal of Remote Sensing*, *18*, 2863–2868.

Pfündel, E., & Bilger, W. (1994). Regulation and possible function of the violaxanthin cycle. *Photosynthesis Research*, *42*, 89–109.

Prince, S. D., & Tucker, C. J. (1986). Satellite remote sensing of rangelands in Botswana: II. NOAA AVHRR and herbaceous vegetation. *International Journal of Remote Sensing*, *7*, 1555–1570.

Rahman, A. F., Gamon, J. A., Fuentes, D. A., Roberts, D., & Prentiss, D. (2001). Modeling spatially distributed ecosystem flux of boreal forests using hyperspectral indices from AVIRIS imagery. *Journal of Geophysical Research*, *106*(D24), 33579–33591.

Roberts, D. A., Green, R. O., & Adams, J. B. (1997). Temporal and spatial patterns in vegetation and atmospheric properties from AVIRIS. *Remote Sensing of Environment*, *62*, 223–240.

Rouse, J. W., Haas, R. W., Schell, J. A., Deering, D. W., & Harlan, J. C. (1974). Monitoring the vernal advancement and retrogadation (Greenwave effect) of natural vegetation. *NASA/GSFC Type III Final Report*, Greenbelt, MD, USA.

Sellers, P. J. (1985). Canopy reflectance, photosynthesis and transpiration. *International Journal of Remote Sensing*, *6*, 1335–1372.

Townshend, J. R. G., & Justice, C. O. (1986). Analysis of the dynamics of the African vegetation using the normalized difference vegetation index. *International Journal of Remote Sensing*, *7*, 1435–1445.

Tucker, C. J., Fung, I. Y., Keeling, C. D., & Gammon, R. H. (1986). Relationship between atmospheric CO_2 variations and a satellite-derived vegetation index. *Nature*, *319*(6050), 195–199.

Ustin, S. L., Roberts, D. A., Pinzon, J. E., Jacquemoud, S., Scheer, G., Castenada, C. M., & Palacios, A. (1998). Estimating canopy water content of chaparral shrubs using optical methods. *Remote Sensing of Environment*, *65*, 280–291.

Vargas-Guzmán, J. A., Myers, D. E., & Warrick, A. W. (2000). Derivatives of spatial variances of growing windows and the variogram. *Mathematical Geology*, *32*(7), 851–871.

Webster, R. (1985). Quantitative spatial analysis of soil in the field. *Advances in Soil Science*, *3*, 1–70.

Webster, R., & Nortcliff, S. (1984). Improved estimation of micronutrients in hectare plots of the Sonning series. *Journal of Soil Science*, *35*, 667–672.

Woodcock, C. E., & Strahler, A. H. (1987). The factor of scale in remote sensing. *Remote Sensing of Environment*, *21*, 311–322.

Woodcock, C. E., Strahler, A. H., & Jupp, D. L. B. (1988). The use of variogram in remote sensing: I. Scene models and simulated images. *Remote Sensing of Environment*, *25*, 323–348.